MAPPING OF FERRIC IRON VARIATION IN LUNAR GLASS BEADS: OBSERVING CHANGING OXIDATION CONDITIONS *IN SITU*. M. C. McCanta[1], M. D. Dyar[2], L. Breitenfield[2], and A. Lanzirotti[3], [1]Dept. of Earth & Planetary Sciences, University of Tennessee, 1621 Cumberland Ave, Knoxville TN 37996 (mmccanta@utk.edu), [2]Planetary Science Institute, 1700 East Fort Lowell, Tucson, AZ 85719, [3]Center for Advanced Radiation Sources (CARS), The University of Chicago, Chicago, IL 60637.

Introduction: Mössbauer reports of Fe^{3+} in lunar glasses and minerals extend back to the time of the missions themselves [e.g., 1,2]. In contrast, petrologic phase equilibria data on returned samples indicate that the oxygen fugacity (f_{O2}) of the lunar interior is ~IW-1, a reduced region where significant Fe^{3+} is not expected [3]. This contradiction persisted for decades until new light was shed on this problem by recent studies [e.g., 4-7] indicating that the Moon is not as dry as previously thought. Given the relationship between oxygen and hydrogen fugacities, this work re-opens the question of the presence of Fe^{3+} in lunar glasses. Results of individual point analyses of lunar picritic glass beads indicate they contain 0-25% Fe^{3+} [8]; several beads display Fe^{3+} zoning profiles consistent with a late-stage oxidation event.

The presence of Fe^{3+} is significant because it records oxygen potential and thus traces the evolution of oxygen through the parameter of f_{O2} in solar system materials. Quantifying f_{O2} in igneous melts is important for constraining planetary interior physical conditions, but also for investigating potential changes during devolatilization-driven eruptive mechanisms. Historically, quantification of Fe^{3+} in glasses required either wet chemistry or Mössbauer spectroscopy, techniques that require large sample sizes and bulk material. Here we present a new synchrotron X-ray absorption spectroscopy (XAS) method for mapping Fe^{3+} *in situ*, enabling resolution of potential variations at micron scales of individual grains or other features in thin sections. Through mapping of lunar glass beads, we are studying changing oxidation conditions during magma ascent and eruption.

Background: Our glass calibration [9] spans 120 different silicate and redox compositions, and permits accurate *in situ* microscale Fe^{3+} measurements with an average accuracy of ±3.6 %, similar to that of Mössbauer when the spectral range covering the Fe *K* absorption pre-edge and main edge (7020-7220 eV) is utilized.

Because acquiring the full spectral range (300-800 data points) is time-consuming, previous work has generally depended upon single point measurements, although linear traverses are possible with limited numbers of points. In such circumstances, relevant spatial information that may be overlooked. To observe all geochemical variations in major and minor elements, element mapping is performed on the electron microprobe, but this has not previously been possible for XAS.

In developing the glass Fe^{3+} calibration noted above, we tested the least absolute shrinkage and selection operator (Lasso) multivariate model. Lasso models are sparse in that they select only the specific channels that explain the most variance in Fe^{3+}. Channels that are judged to be less informative are eventually omitted from the regression equation altogether in an iterative process, making the lasso more robust against noise than other approaches such as partial least-squares.

For example, the vertical red lines in Figure 1 represent the 31 channels chosen by the Lasso for use in the expression to predict Fe^{3+} in garnet with an error bar of ±0.01%. Maps of garnet Fe^{3+} can be produced by collecting data only on those 31 channels instead of all 600 – a dramatic time reduction that allows relatively dense maps of Fe^{3+} to be produced. The number of Lasso coefficients for Fe^{3+} in any model can be tuned to balance prediction accuracy with analysis time.

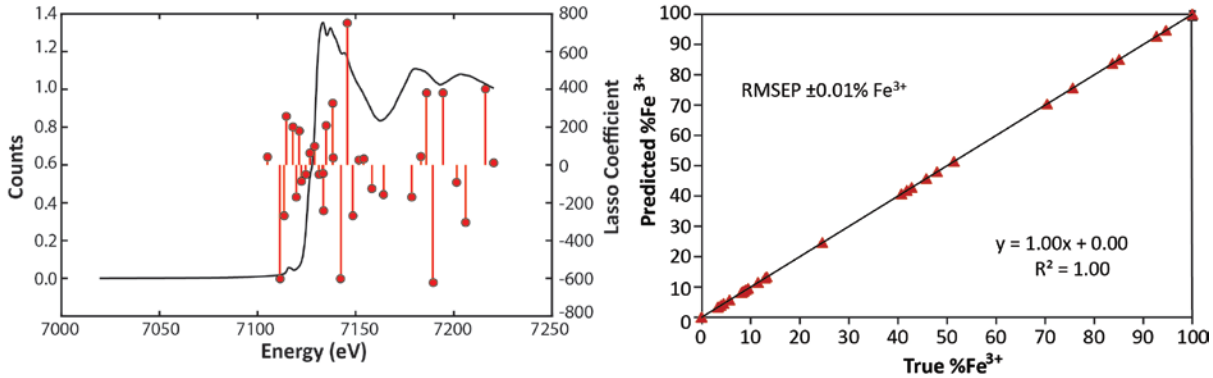

Figure 1. (left) A typical garnet XAS spectrum (in black) with the locations and magnitudes of lasso coefficients shown as vertical red lines that represent the channels where information needed to predict Fe^{3+} is located. (right) Graph of predicted vs. measured by Mössbauer Fe^{3+} contents of garnet standards using the only the 31 channels noted in the left panel.

Analytical Methods: Major and minor element concentrations in 27 lunar glass beads from Apollo 11 (10084), 14 (14148), and 17 (74220) were analyzed on the Brown University Cameca SX-100 electron probe. XAS Fe^{3+} maps were collected at beamline 13-IDE at the Advanced Photon Source at Argonne National Lab using a 1 μm spot size. 50×50 pixel grids were set up to cover the glass bead with analyses taking ~2 hours per map. Spectral channels for maps were selected based on a Lasso model tuned on 369 glass standard spectra [9] to produce only 4 coefficients by setting the α (adjustable parameter) value to 0.1. The Data Exploration, Visualization, and Analysis for Spectroscopy (DEVAS) website (nemo.cs.umass.edu:54321) was used to create a Lasso model for which the resultant prediction equation, $\%Fe^{3+}=-30\times I_{7118.5}-143\times I_{7123.5}+46\times I_{7132.5}+129\times I_{7219}$ hadh an internal cross-validation error of ±11% absolute. At this level of accuracy, maps can be expected to be qualitative only, but they provide a rapid means of identifying cadidates for subsequent full-spectra analyses at spot locations. Two additional channels in the pre-edge region were also sampled to reflect pre-edge centroids for Fe^{2+} (7111.85 eV) and Fe^{3+} (7113.7 eV), totaling six analyses per pixel.

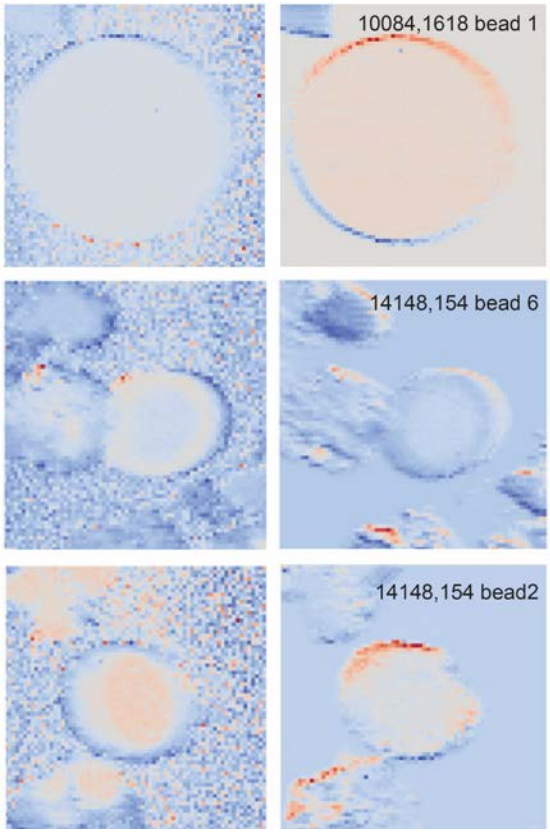

Figure 2. Maps of Fe^{3+} contents in lunar glass beads from 10084 and 14148 – blue is high Fe^{3+} and orange is low. Top row shows an unzoned sample. Middle and bottom rows show samples with opposite zoning. Left column is the ratio of $I_{7111.85}/I_{7113.7}$ and right shows the results of using the 4-channel expression $-30\times I_{7118.5}-143\times I_{7123.5}+46\times I_{7132.5}+129\times I_{7219}$.

Maps were built using the GSE Mapviewer software created using the Python-based Larch open-source library toolkit for processing and analyzing X-ray spectroscopic and scattering data from synchrotrons (http://cars.uchicago.edu/xraylarch/). It allows visualization and analysis of micro-x-ray flurescence maps. For each of the 32 glass beads analyzed, maps were created using two different metrics: 1) the Lasso expression given above and 2) the ratio of the peak intensity at 7111.85 eV to that at 7113.7 eV.

Results: Following the results of our earlier point analysis work, many of the beads analysed showed no evidence of Fe^{3+} variations (10084, Fig. 2) [8]. However, five beads were observed to have measureable differences in Fe^{3+} (14148, Fig. 2) for both analytical metrics. These included zoning from reduced to oxidized and the reverse, as well as patchy zoning.

Discussion: The occurrence of unzoned beads and beads with both oxidized and reduced rims can best be explained by considering late-stage magma ascent and eruption conditions. A late-stage oxidation event (Stage 3 in [10]), observed in Ni-rich rims on metal grains in the glass beads, likely results from loss of water from the ascending melt [10]. This produces melt oxidation through the reaction: $4OH=H_2O+H_2+1.5O_2$. Redox kinetic calculations suggest that oxidation of a melt droplet under these conditions takes place in under 1 s [8]. Although the unzoned beads have no Fe^{3+} variations, they do contain significant amounts of Fe^{3+} (up to 28% of total Fe) [8] consistent with this oxidation event. Oxidation takes place from the rim inward. Therefore, zoned beads with oxidized rims (Fig. 2, middle) represent incomplete oxidation prior to the closure temperature. Zoned beads with reduced rims (Fig. 2, bottom) likely represent subsequent reduction either in the lunar vacuum or in the dissipating gas cloud that may have been fairly reducing due to the addition of H from the degassing melt.

Acknowledgments: We are grateful for support from NASA grant NNX16AR18G.

References: [1] Finger 1972, Carn. Year. 71, 600-603. [2] Schürmann & Hafner 1972, Proc. Lunar Sci. Conf. 3, 615-621. [3] Sato 1976, Proc. Lunar Sci. Conf. 7, 1323-1344. [4] Saal et al. 2008, Nature 454, 192-196. [5] McCubbin et al. 2010, Amer. Mineral. 95, 1141-1150. [6] Hauri et al. 2011, Science 333, 213-215. [7] Wetzel et al. 2015, Nature Geosci. 8, 755-758. [8] McCanta et al. 2017, Icarus 285, 95-102. [9] Dyar et al. 2016, Amer. Mineral. 101, 744-748. [10] Rutherford et al 2017, Amer. Mineral. 102, 2045-2053.